analytical chemistry

pubs.acs.org/ac Article

Low-background Near-infrared Fluorescent Probe for Real-time Monitoring of β-Glucuronidase Activity in Inflammation and Therapy

Dianfeng Dai, Zhimin Zhang, Mo Ma, Chen Zhao, Jingkang Li, Siqi Zhang, Pinyi Ma,* Qiong Wu,* and Daqian Song*

Cite This: *Anal. Chem.* 2025, 97, 9414−9421 Read Online

ACCESS | Metrics & More | Article Recommendations | Supporting Information

ABSTRACT: β-Glucuronidase (GUS) is an acidic hydrolase enzyme overexpressed in various inflammatory diseases, making it a promising biomarker for inflammation. However, current tools for real-time, *in situ* imaging of GUS activity are hindered by background interference, which reduces their effectiveness in dynamic biological environments. To address this challenge, we developed Ox-GUS, a GUS-specific fluorescent probe with a unique molecular design featuring a disrupted conjugated structure. This design provided Ox-GUS with near-zero background optical properties, a significantly enhanced signal-to-noise ratio, and a highly sensitive detection ability. The probe demonstrated a fluorescence enhancement of up to 400 folds in response to GUS activity, with a detection limit as low as 0.0035 U/mL. We successfully employed Ox-GUS to visualize GUS activity in real-time in mouse models of rheumatoid arthritis, autoimmune hepatitis, and inflammatory bowel disease, and effectively monitored therapeutic responses. This study highlights the potential of Ox-GUS as a robust tool for advancing research on GUS-related inflammatory mechanisms and for early diagnosis and treatment monitoring of inflammatory diseases.

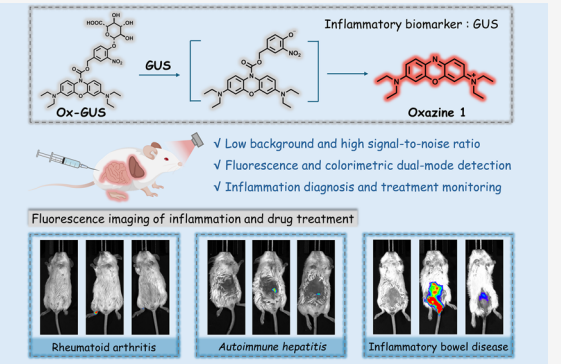

INTRODUCTION

Inflammation is a complex biological response triggered by infection, injury, or harmful stimuli, aimed at eliminating pathogenic factors and initiating tissue repair.[1−5] Biomarkers of inflammatory diseases play a pivotal role in understanding the severity and progression of inflammation, providing critical insights into the molecules and pathways involved.[6−9] Real-time monitoring of these markers can greatly enhance early diagnosis and therapeutic management by delivering dynamic and precise information on disease progression.[10−13]

β-glucuronidase (GUS), an acidic hydrolase enzyme, is central to various biological processes, including cellular detoxification and metabolic waste clearance.[14−17] Notably, GUS is overexpressed in inflammatory diseases such as arthritis, hepatitis, and pancreatitis, establishing it as a valuable biomarker for inflammation.[18−21] Despite its importance, current methods for detecting GUS activity rely primarily on *ex vivo* analyses of blood or tissue samples.[22,23] These approaches are time-consuming, labor-intensive, and prone to inaccuracies due to sample processing, which limits their utilization in real-time, dynamic *in vivo* analyses.[24−27]

Fluorescent probes have emerged as powerful tools for *in situ* detection of biomarker activity.[6,28−30] β-glucuronide is a recognition group commonly used in GUS-targeted fluorescent probes, and numerous probes have been developed using this group.[31,32] For example, Feng et al. developed HC-glu for the detection of GUS activity in the intestines of animals such as mice and zebrafish.[33] Ding et al. introduced DP-GLU to noninvasively track GUS levels in a mouse tumor model.[34] Liu et al. designed DCDNO2, a fluorescent probe for imaging and detecting hepatocellular carcinoma cells and tumor tissues in mice.[35] The probe can also be used in conjunction with real-time imaging to guide surgical resection of liver cancer tumors. However, these probes predominantly rely on internal charge transfer (ICT) mechanisms induced by their recognition group. This often leads to incomplete fluorescence quenching and high background signals. Consequently, traditional GUS-targeted fluorescent probes suffer from substantial background interference, which reduces their effectiveness in complex biological environments. These limitations significantly hinder their use for real-time imaging and dynamic analysis,

Received: January 28, 2025
Revised: March 31, 2025
Accepted: April 16, 2025
Published: April 24, 2025

https://doi.org/10.1021/acs.analchem.5c00658
Anal. Chem. 2025, 97, 9414−9421

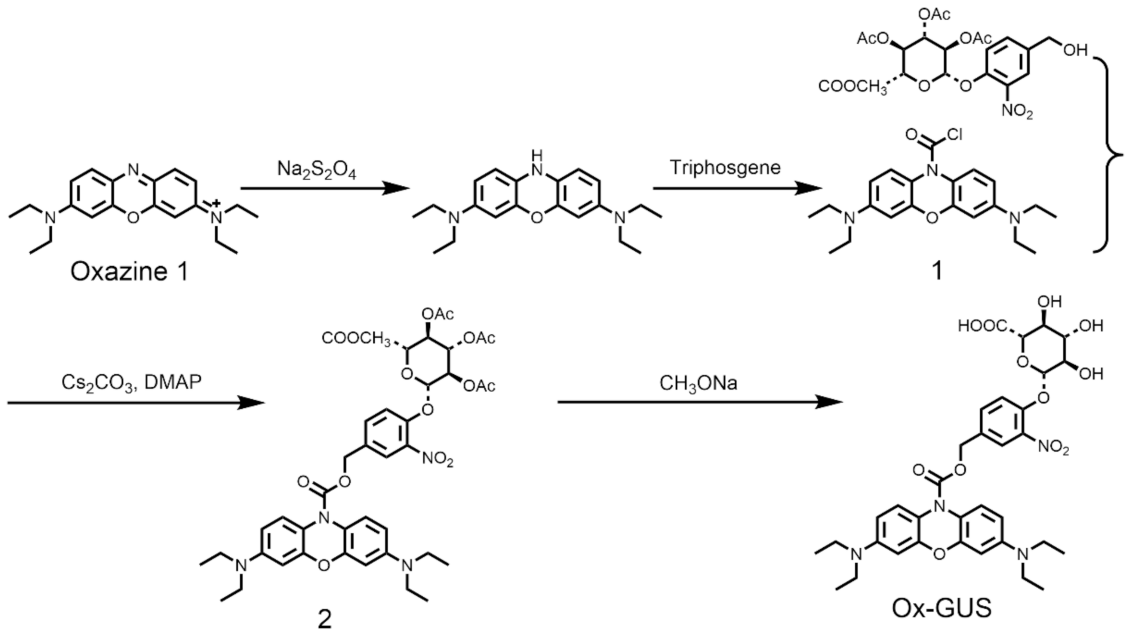

Figure 1. Synthesis route of Ox-GUS.

particularly *in vivo* analysis, where high sensitivity and specificity are essential.[36,37]

Although the association between β-glucuronidase and inflammation has been discovered, no fluorescent probe has been developed to date that enables real-time in situ visualization of GUS activity across different inflammatory tissues, which greatly limits further investigation of GUS as a biomarker for inflammatory diseases (Table S1). To overcome these challenges, we designed and synthesized Ox-GUS, a GUS-specific fluorescent probe. Ox-GUS consists of three key components: (1) oxazine 1 as the fluorophore, (2) 4-hydroxymethyl-2-nitrophenol as the linker group, and (3) β-glucuronide as the recognition group. The disrupted conjugated structure of Ox-GUS effectively minimizes spectral background interference, resulting in near-zero background fluorescence and a dramatically improved signal-to-noise ratio. In addition, we incorporated a connecting group, as reported by Liu et al., by introducing a $-NO_2$ group onto 4-hydroxybenzyl alcohol.[35] This modification enhances the efficiency of glycosidic bond cleavage in the presence of GUS, further improving the probe's responsiveness. The unique design of Ox-GUS allows it to detect β-glucuronidase activity with high sensitivity using both fluorescence and colorimetry methods. Ox-GUS was applied in real-time, *in situ* fluorescence imaging of GUS activity at inflammatory sites in various mouse models of inflammatory diseases, including rheumatoid arthritis, autoimmune hepatitis, and inflammatory bowel disease. This probe shows potential as a tool for monitoring dynamic changes in GUS activity under diverse physiological and pathological conditions, as well as during therapeutic interventions. Overall, the developed probe can be utilized as a versatile tool for monitoring and detecting inflammation-related processes.

EXPERIMENTAL SECTION

Materials and Instruments. The chemicals, reagents, and analytical instruments are detailed in the Supporting Information.

Synthesis. The synthetic route for Ox-GUS is presented in Figure 1. The preparation of Compound 1 was carried out following a previously reported method.[36]

Synthesis of Compound 2. Under a nitrogen atmosphere, (2S,3R,4S,5S,6S)-2-(4-(hydroxymethyl)-2-nitrophenoxy)-6-(methoxycarbonyl)tetrahydro-2H-pyran-3,4,5-triyl triacetate (194 mg, 0.4 mmol), Compound 1 (155 mg, 0.4 mmol), Cs_2CO_3 (391 mg, 1.2 mmol), and DMAP (49 mg, 0.4 mmol) were mixed with 30 mL of dichloromethane and incubated overnight at 45 °C. The reaction mixture was washed three times with 50 mL of 1 M HCl, and the solvent was removed under reduced pressure. The crude product was purified by silica gel column chromatography and eluted with dichloromethane/methanol (*v*/*v*, 30:1), from which Compound 2 as a white solid (64 mg, 19% yield) was obtained. ^{1}H NMR (600 MHz, $CDCl_3$) δ 7.85 (d, J = 2.0 Hz, 1H), 7.56 (dd, J = 8.6, 2.1 Hz, 1H), 7.35 (d, J = 8.6 Hz, 1H), 7.30 (d, J = 8.0 Hz, 2H), 6.50 − 6.25 (m, 4H), 5.38 − 5.27 (m, 3H), 5.26 − 5.17 (m, 3H), 4.21 (d, J = 8.9 Hz, 1H), 3.74 (s, 3H), 3.32 (q, J = 6.8 Hz, 8H), 2.12 (s, 3H), 2.06 (d, J = 5.1 Hz, 6H), 1.15 (t, J = 6.9 Hz, 12H) (Figure S1). ^{13}C NMR (151 MHz, $CDCl_3$) δ 170.02, 169.31, 169.26, 166.68, 151.22, 148.70, 146.59, 141.23, 133.37, 124.98, 124.70, 120.11, 120.00, 116.79, 111.60, 106.43, 99.82, 99.48, 72.58, 71.15, 70.20, 68.75, 65.72, 53.05, 44.58, 20.60, 20.56, 20.52, 12.55 (Figure S2). HR-MS (m/z): Calculated for $[C_{41}H_{50}N_4O_{15}]^{2+}$: 419.1631, found: 419.1629 (Figure S3).

Synthesis of Ox-GUS. Compound 2 (54 mg, 0.065 mmol) and sodium methoxide (7.02 mg, 0.13 mmol) were dissolved in 4 mL of methanol, and the mixture was stirred at room temperature for 1.5 h. The reaction mixture was concentrated under reduced pressure to remove the solvent. The crude product was purified by silica gel column chromatography and eluted with dichloromethane/methanol (v/v, 10:1) to obtain Ox-GUS as a white solid (19 mg, 42% yield). ^{1}H NMR (600 MHz, DMSO-d_6) δ 8.48 (s, 1H), 7.90 (s, 1H), 7.67 (d, J = 8.7 Hz, 1H), 7.44 (d, J = 8.7 Hz, 1H), 7.30 (d, J = 8.9 Hz, 2H), 6.40 (d, J = 9.0 Hz, 2H), 6.33 (s, 2H), 5.32 (t, J = 4.8 Hz, 1H), 5.20 (s, 2H), 5.10 (d, J = 7.5 Hz, 1H), 3.51 (s, 2H), 3.31 (d, J = 7.0 Hz, 8H), 3.16 (d, J = 7.9 Hz, 1H), 3.09 (d, J = 5.1 Hz,

https://doi.org/10.1021/acs.analchem.5c00658
Anal. Chem. 2025, 97, 9414−9421

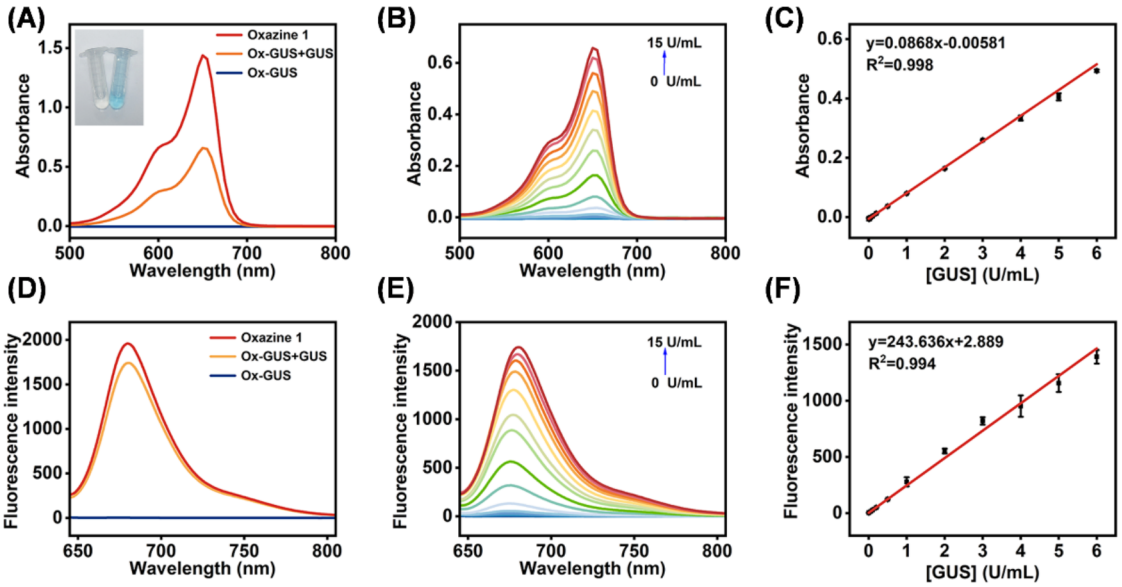

Figure 2. (A) Absorption spectra of Ox-GUS (10 μM), the reaction system (10 μM Ox-GUS + 15 U/mL GUS), and oxazine 1 (10 μM). The illustration shows the color change of the reaction system without GUS (left) and with GUS (right). (B) Absorption spectra of Ox-GUS (10 μM) in the presence of GUS at different concentrations (0−15 U/mL). (C) Linear relationship between absorbance at 650 nm and GUS concentration (0−6 U/mL). (D) Fluorescence spectra of Ox-GUS (10 μM), the reaction system (10 μM Ox-GUS + 15 U/mL GUS), and oxazine 1 (10 μM). (E) Fluorescence spectra of Ox-GUS (10 μM) in the presence of GUS at different concentrations (0−15 U/mL). (F) Linear relationship between fluorescence intensity (λ_{ex} = 635 nm) and GUS concentration (0−6 U/mL).

1H), 3.03 − 2.99 (m, 2H), 1.07 (t, J = 6.9 Hz, 12H) (Figure S4). ^{13}C NMR (151 MHz, DMSO-d_6) δ 172.35, 153.34, 151.21, 149.96, 146.59, 140.10, 134.03, 130.12, 125.63, 124.57, 117.65, 116.80, 106.74, 100.71, 99.17, 77.23, 74.08, 73.47, 72.26, 66.36, 44.22, 12.85 (Figure S5). HR-MS (m/z): Calculated for $[C_{34}H_{42}N_4O_{12}]^{2+}$: 349.1394, found: 349.1391 (Figure S6).

***In Vitro* Detection of GUS.** Ox-GUS was dissolved in DMSO to prepare a 1 mM stock solution. In GUS detection, a reaction system containing Ox-GUS (10 μM) and PBS (10 mM, pH 7.4) was prepared at a final volume of 1 mL. The UV−visible absorption spectra and fluorescence spectra of the reaction system were recorded using a UV−visible spectrophotometer and fluorescence spectrometer, respectively. The stock solution was stored at −20 °C.

Cell Imaging. Cells in the blank control group did not receive any treatment. To study GUS expression, cells were treated with Ox-GUS (10 μM) for 50 min. To study inflammatory GUS expression, cells were treated with LPS (0.5 μg/mL) for 24 h, followed by Ox-GUS (10 μM) for 50 min. To investigate endogenous GUS regulation during inflammation, cells were treated with LPS (0.5 μg/mL) for 24 h, followed by baicalin (200 μM) for 1 h, and then Ox-GUS (10 μM) for 50 min. Prior to imaging, all cells were washed three times with PBS (10 mM, pH 7.4). Fluorescence signals were then collected using a laser scanning confocal microscope.

Fluorescence Imaging of Mouse Models. All animal experiments have been approved by the Institutional Animal Care and Use Committee (IACUC) of Jilin University (ethical review permit number SY2024090007). The experiments were conducted in compliance with established ethical protocols to minimize animal distress.

Rheumatoid Arthritis Model. Mice in the inflammation group were injected with λ-carrageenan (10 mg/mL, 50 μL PBS) in the right tibial joint. Mice in the treatment group received an intra-articular injection of methotrexate (1 mg/mL, 50 μL) in the same joint 4 h after λ-carrageenan injection. Mice in the control group received an equivalent volume of normal saline. Seven hours after the treatment, all mice were subcutaneously injected with Ox-GUS (200 μM, 50 μL) in the right tibial joint. Mice were anesthetized using isoflurane and imaged *in vivo* using a small animal imaging system 10 min after injection.

Autoimmune Hepatitis Model. To establish an autoimmune hepatitis mouse model, mice in the inflammation group received concanavalin A (ConA, 20 mg/kg) via tail vein injection. Mice in the treatment group were injected intraperitoneally with prednisolone (10 mg/kg) 30 min after ConA injection. Mice in the control group were injected with an equivalent volume of normal saline. Twelve hours after the treatment, all mice were injected with Ox-GUS (200 μM, 100 μL) via the tail vein. Ten minutes after injection, mice were anesthetized using isoflurane and then imaged using a small animal imaging system. After imaging, major organs were collected for *ex vivo* fluorescence imaging.

Inflammatory Bowel Disease Model. To establish an inflammatory bowel disease (IBD) mouse model, mice in the inflammation group were provided with drinking water containing 5% dextran sulfate sodium (DSS). Treatment group mice were gavaged daily with cyclosporin A (25 mg/kg) starting on the same day as DSS administration. Control group mice were fed with a standard diet and drinking water. After 7 days, all mice were anally injected with Ox-GUS (200 μM, 100 μL). Mice were anesthetized using isoflurane and subjected to imaging using a small animal imaging system 10 min after injection. After imaging, major organs were collected and subsequently subjected to ex vivo fluorescence imaging.

https://doi.org/10.1021/acs.analchem.5c00658
Anal. Chem. 2025, 97, 9414−9421

RESULTS AND DISCUSSION

Optical Response of Ox-GUS to GUS. The changes in UV−vis and fluorescence spectra of Ox-GUS before and after its reaction with GUS were first investigated. Before the addition of GUS, Ox-GUS was colorless and transparent and exhibited minimal UV absorption and fluorescence. This indicates that Ox-GUS nearly does not exhibit background signals. Upon the addition of GUS, the solution color turned from colorless to blue. Distinct UV−vis absorption and fluorescence emission peaks also appeared at 650 and 680 nm, respectively (Figure 2A,2D). The reaction conditions for Ox-GUS were then optimized. The fluorescence intensity reached its peak at 1 h (Figure S7). All spectral tests were performed in PBS (10 mM, pH 7.4) at 37 °C to simulate physiological conditions (Figures S8 and S9).

Dual-modal Detection of GUS. Ox-GUS had excellent performance in dual-modal, quantitative fluorescence and colorimetric detection of GUS. As the GUS concentration increased from 0 to 15 U/mL, the UV−vis absorption peak at 650 nm and the fluorescence emission peak at 680 nm were significantly enhanced (Figure 2B,2E). Notably, Ox-GUS exhibits near-zero spectral background signals and achieves up to 400-fold fluorescence enhancement, significantly higher than other GUS probes while offering excellent signal-to-noise ratio (Table S1). A good linear relationship was observed between the signal enhancement in both detection modes and GUS concentrations within the range of 0 to 6 U/mL. The detection limits were determined to be 0.0049 U/mL for the colorimetric method (Figure 2C) and 0.0035 U/mL for the fluorescence method (Figure 2F). The dual-modal detection capability of Ox-GUS allows for highly sensitive detection of GUS. It also improves the reliability and accuracy of the analysis by providing complementary validation of colorimetric and fluorescence signals. This dual-modal approach provides a more comprehensive method for quantitative analysis.

Photostability and Selectivity. The photostability and selectivity of Ox-GUS were also determined to assess its potential for practical applications. After continuous irradiation with 635 nm light for 1 h, the fluorescence intensity of the reaction system and the probe remained stable, an indication of their good photostability (Figure S10). Common substances in the human body were selected as potential interferents, and their effects on the probe were examined. The fluorescence intensity was almost unchanged after the probe was coincubated with these substances. This confirms that Ox-GUS is highly selective to GUS and suitable for use in complex biological environments (Figure S11).

Enzymatic Reaction Kinetics. The interaction between Ox-GUS and GUS was examined based on their enzymatic reaction kinetics. The Michaelis constant (K_m) for the Ox-GUS-GUS interaction was determined to be 6.2832 μM, indicating a strong binding affinity between them (Figures S12 and S13).

Sensing mechanism. The mechanism of Ox-GUS in detecting GUS was explored using mass spectrometry and molecular docking. Mass spectrometry revealed ion peaks corresponding to both the probe and the fluorophore in the Ox-GUS-GUS reaction system (Figures S6, S14, and S15). Molecular docking results suggested that Ox-GUS formed hydrogen bonds with five specific amino acids—ASP172, GLU425, TYR485, TRP561, and ARG574—at the active site of GUS, with a binding energy of −8.0 kcal/mol. This indicates a strong and stable binding between the probe and the enzyme, involving five hydrogen bonds (Figure S16). Based on these findings, the sensing mechanism was proposed: (1) GUS specifically cleaves the β-glucuronide moiety from the probe; (2) this cleavage triggers the self-immolation of the linker group in Ox-GUS; and (3) as a result, the fluorophore (oxazine 1) is released, producing a detectable fluorescence signal.

Fluorescence Imaging of GUS Activity in Living Cells. Before live cell fluorescence imaging, the cytotoxicity of Ox-GUS was tested on HepG2 cells using the CCK8 assay. The results showed that Ox-GUS at concentrations ranging from 10 to 100 μM had negligible effects on cell viability, indicating it has good biocompatibility (Figure S17).

Ox-GUS was then applied for fluorescence imaging in HepG2 cells. The optimal incubation time for the cells and the probe was determined. The fluorescence intensity was found to gradually increase with time and reached its maximum value at 50 min. Thus, 50 min was chosen as the optimal incubation time (Figure S18). Since β-glucuronidase is located in cellular lysosomes, we investigated the intracellular distribution of Ox-GUS through lysosomal colocalization experiments. As shown in Figure S19, the red fluorescence from Ox-GUS demonstrated strong overlap with green fluorescence from the commercial lysosomal dye (LysoTracker Green), yielding a Pearson correlation coefficient of 0.90. These results indicate that Ox-GUS primarily localizes in lysosomes, enabling accurate in situ visualization of intracellular GUS. To visualize changes in GUS activity during an inflammatory response at the cellular level, an LPS-induced inflammation model was established. The results showed that the fluorescence intensity of LPS-treated cells was markedly higher than that of the control group (untreated cells), suggesting GUS expression was elevated during inflammation. To confirm that the increase in fluorescence intensity was due to elevated endogenous GUS levels, LPS-induced inflammatory cells were treated with baicalin, a GUS-specific inhibitor. The addition of baicalin significantly reduced the red fluorescence of the cells (Figure 3A,3B). This finding confirmed that the increased fluorescence was due to higher GUS expression in inflammatory cells. These results demonstrate that Ox-GUS can accurately detect changes in GUS levels at the cellular level.

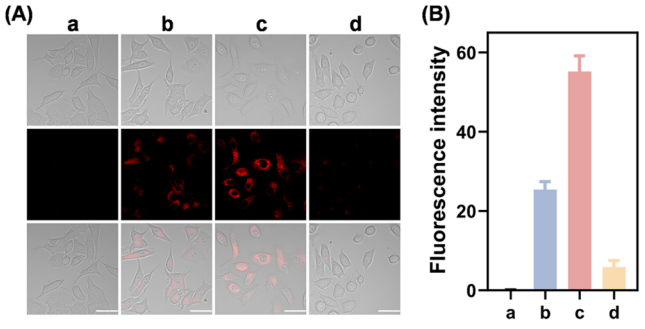

Figure 3. (A) Fluorescence imaging of HepG2 cells under different treatment conditions: (a) untreated cells; (b) cells incubated with Ox-GUS (10 μM) for 50 min; (c) cells incubated with LPS (0.5 μg/mL) for 24 h, followed by Ox-GUS (10 μM) for 50 min; (d) cells incubated with LPS (0.5 μg/mL) for 24 h, followed by baicalin (200 μM) for 1 h, and Ox-GUS (10 μM) for 50 min. (λ_{ex} = 640 nm, λ_{em} = 663−738 nm. Scale bar = 50 μm). (B) Comparison of fluorescence intensities for the different treatments in (A).

https://doi.org/10.1021/acs.analchem.5c00658
Anal. Chem. 2025, 97, 9414−9421

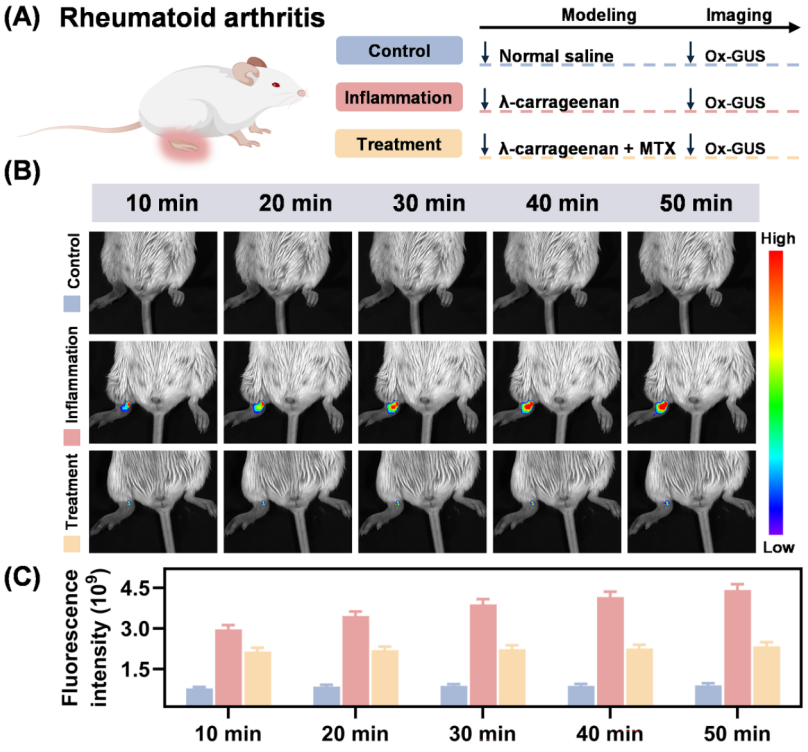

Figure 4. (A) Schematic diagram showing the procedure for developing RA mouse model used for *in vivo* fluorescence imaging. (B) Fluorescence images of mice in the control group, inflammation group, and treatment group at different time points after Ox-GUS injection. (C) Mean fluorescence intensity of images in (B).

Fluorescence Imaging of GUS Activity in RA Mouse Model. Rheumatoid arthritis (RA) is an autoimmune disease characterized by synovitis, which leads to the destruction of articular cartilage and bone.[38] This progression ultimately causes joint deformities and loss of function.[38] Traditional imaging techniques such as X-ray, CT, MRI, and ultrasound have been widely used to detect RA.[39] However, they primarily focus on structural changes in bones and joints and fail to capture dynamic molecular changes at the pathological level.[39] This limits their ability to elucidate pathological processes underlying RA. Although studies have found increase of GUS expression in RA, no diagnostic tools have been developed to utilize this feature for RA diagnosis and therapeutic monitoring.[40,41] To address this limitation, we utilized Ox-GUS to visualize changes in GUS expression during RA progression. RA models were established by injecting λ-carrageenan into the right tibial joint of mice, followed by Ox-GUS administration (Figure 4A). Fluorescence imaging revealed a progressive increase in fluorescence in the joints of mice over time after probe injection. Notably, fluorescence in the joints of RA mice was significantly stronger than that of the control mice, indicating markedly elevated GUS expression during RA progression. Additionally, we evaluated GUS expression during RA treatment using methotrexate, a commonly used clinical drug. The results demonstrated a notable reduction in fluorescence in the joints of treated mice, suggesting that methotrexate effectively decreased GUS expression in inflamed joints (Figure 4B,4C). These findings demonstrate that Ox-GUS can dynamically monitor GUS activity in joints, providing valuable insights for both diagnostic and therapeutic evaluation of RA. In summary, GUS levels are elevated during RA progression, and Ox-GUS can monitor GUS activity in joints in real-time. This approach provides a new perspective for studying RA pathology and has potential as a simple and rapid tool for RA diagnosis and therapeutic efficacy evaluation.

Fluorescence Imaging of GUS Activity in AIH Mouse Model. Autoimmune hepatitis (AIH) is a chronic inflammatory liver disease resulting from an abnormal immune reaction against liver cells, which leads to liver damage.[42] Because AIH often has an insidious onset and is asymptomatic in its early stages, it frequently progresses unnoticed until significant liver damage has occurred.[43] To study GUS activity in liver inflammation, a ConA-induced mouse model was used to simulate AIH. After successfully establishing the mouse model, Ox-GUS was injected in the mice, and *in vivo* fluorescence imaging was performed 10 min later (Figure 5A). The results showed a significant increase in fluorescence intensity of the inflammation group compared to negligible fluorescence observed in the control group. This observation indicates that GUS expression is elevated in the liver of AIH mice. To further assess the ability of Ox-GUS to evaluate therapeutic effects, we used prednisolone, a clinically prescribed drug for AIH treatment. The results showed that the fluorescence intensity of the treatment group was significantly reduced, confirming that the treatment with prednisolone could lower GUS levels in the liver (Figures 5B and 5C). *Ex vivo* fluorescence imaging of major organs also showed similar results: the liver of AIH mice exhibited strong fluorescence, while that of the treatment group exhibited notably lower fluorescence (Figure 5D). H&E staining further confirmed hepatic tissue necrosis and inflammatory infiltration in AIH mice, and the treatment with prednisolone could alleviate these symptoms (Figure 5E). In conclusion, during AIH inflammation, liver GUS activity is elevated. Additionally, Ox-GUS can effectively monitor the progression of AIH and the therapeutic

https://doi.org/10.1021/acs.analchem.5c00658
Anal. Chem. 2025, 97, 9414−9421

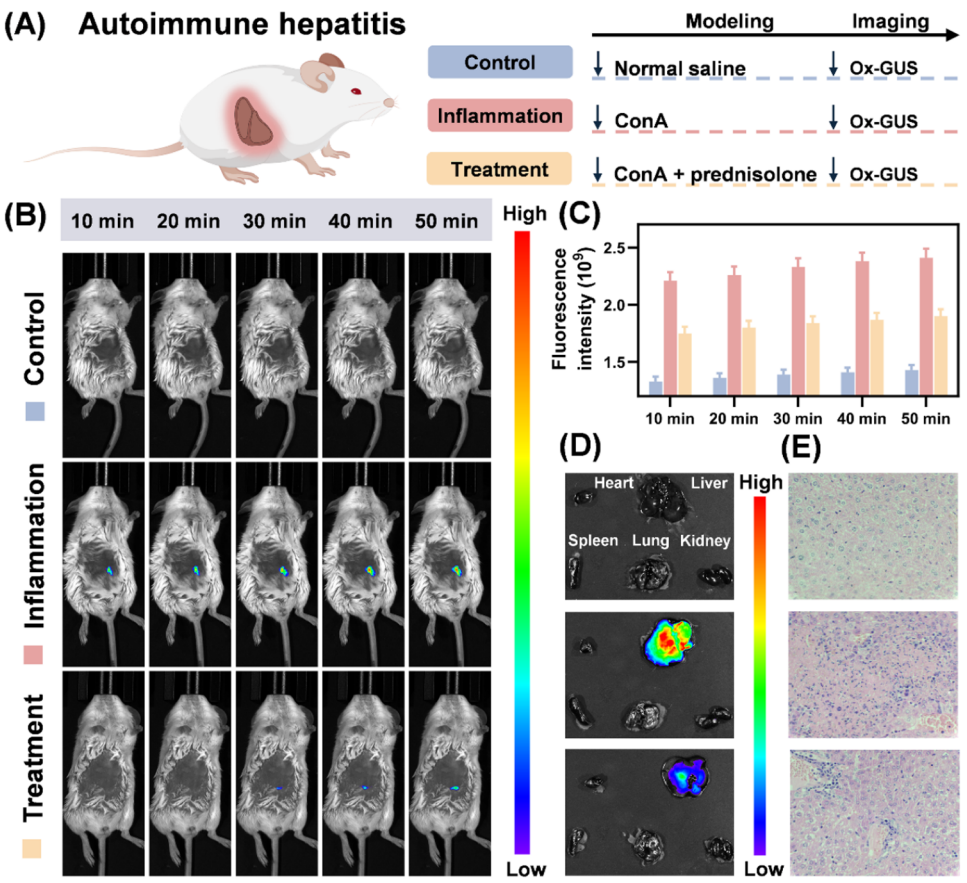

Figure 5. (A) Schematic diagram showing the procedure for developing AIH mouse model used for *in vivo* fluorescence imaging. (B) Fluorescence images of mice in the control group, inflammation group, and treatment group at different time points after Ox-GUS injection. (C) Mean fluorescence intensity of images in (B). (D) Fluorescence images of dissected organs of mice in the control group, inflammation group, and treatment group. (E) H&E staining images of liver tissue of mice in the control group, inflammation group, and treatment group (×400 magnification).

effects of treatment. Thus, it could be used as a novel diagnostic tool for early detection and evaluation of liver inflammatory diseases.

Fluorescence Imaging of GUS Activity in IBD Mouse Model. Inflammatory bowel disease (IBD) is a chronic, relapsing inflammatory condition of the intestine that significantly affects the quality of life of patients and increases the risk of colorectal cancer.[44] Accurate diagnosis and effective treatment during inflammatory episodes are crucial for preventing disease progression and improving prognosis.[45] To address these needs, we used Ox-GUS to monitor GUS activity in an IBD mouse model induced by dextran sulfate sodium (DSS) (Figure 6A). Fluorescence imaging showed a gradual increase in fluorescence intensity over time in the inflammation group, and the intensity was notably higher in comparison to the control group, indicating elevated GUS expression during IBD. These findings suggest that Ox-GUS can serve as a fluorescence tool for diagnosing IBD. We also evaluated the therapeutic effect of cyclosporin A (CsA), a drug used to treat IBD. The results showed that the fluorescence intensity of the treatment group was significantly lower compared to the IBD model group. This indicates that CsA treatment decreases GUS activity during inflammation (Figure 6B,6C). *Ex vivo* imaging of the organs further confirmed that the intestines of mice in the inflammation group exhibited the brightest fluorescence, consistent with the *in vivo* imaging results (Figure 6D). H&E staining revealed significant inflammatory cell infiltration and goblet cell destruction in the intestines of IBD mice, and CsA treatment markedly alleviated these symptoms (Figure 6E). In summary, through variations in fluorescence intensity, Ox-GUS can accurately reflect dynamic changes in GUS activity during IBD. It can also serve as a reliable tool for evaluating drug efficacy, offering new insights into the clinical management of IBD. These findings highlight the potential of Ox-GUS as an essential tool for diagnosing and assessing the therapeutic effects of IBD treatments.

CONCLUSIONS

In summary, we developed Ox-GUS, a GUS-specific fluorescent probe with exceptional optical properties, including near-zero background fluorescence and absorption. These characteristics resulted in a high signal-to-noise ratio, enabling highly sensitive detection of GUS activity through both fluorescence and colorimetric methods. Ox-GUS could effectively visualize the upregulation of GUS during cellular inflammation. *In vivo* fluorescence imaging confirmed that the probe could sensitively detect changes in GUS activity in inflammatory tissues. This was validated in mouse models of rheumatoid arthritis, autoimmune hepatitis, and inflammatory bowel disease. Additionally, Ox-GUS was able to successfully monitor the decrease in GUS levels following targeted treatment, which highlights its potential for therapeutic

https://doi.org/10.1021/acs.analchem.5c00658
Anal. Chem. 2025, 97, 9414−9421

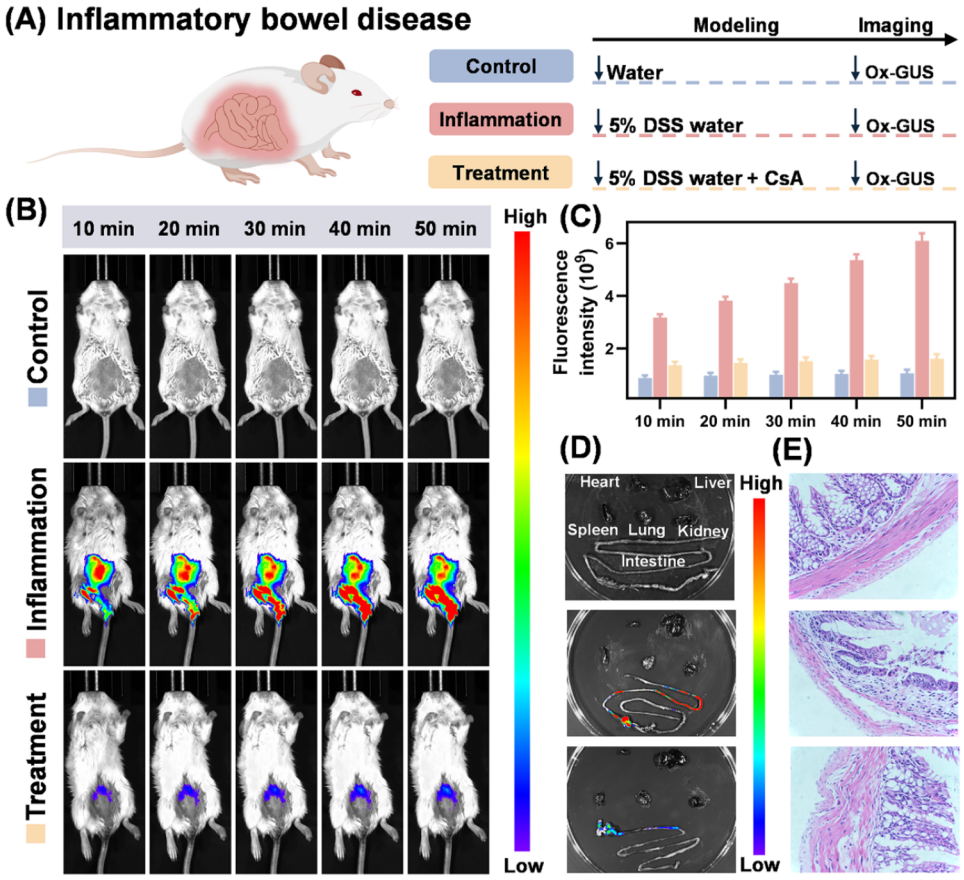

Figure 6. (A) Schematic diagram showing the procedure for developing IBD mouse model used for *in vivo* fluorescence imaging. (B) Fluorescence images of mice in the control group, inflammation group, and treatment group at different time points after Ox-GUS injection. (C) Mean fluorescence intensity of images in (B). (D) Fluorescence images of dissected organs of mice in the control group, inflammation group, and treatment group. (E) H&E staining images of intestine tissue of mice in the control group, inflammation group, and treatment group (×400 magnification).

evaluation. This study shows that Ox-GUS is a powerful tool for investigating the dynamic role of GUS in inflammatory processes. Its application paves the way for advancements in the early diagnosis and treatment monitoring of inflammation-related diseases and reinforces the potential of GUS as a reliable biomarker for inflammatory conditions.

■ ASSOCIATED CONTENT

Supporting Information

The Supporting Information is available free of charge at https://pubs.acs.org/doi/10.1021/acs.analchem.5c00658.

Additional experimental details, including materials and instruments, determination of the detection limit, enzymatic kinetics assays, molecular docking, CCK8 assay, cell culture, and supplementary figures (PDF)

■ AUTHOR INFORMATION

Corresponding Authors

Pinyi Ma − *College of Chemistry, Jilin Province Research Center for Engineering and Technology of Spectral Analytical Instruments, Jilin University, Changchun 130012, China*; orcid.org/0000-0002-3230-4928; Email: mapinyi@jlu.edu.cn

Qiong Wu − *Key Laboratory of Pathobiology, Ministry of Education, Nanomedicine and Translational Research Center, The Third Bethune Hospital of Jilin University, Changchun 130033, China*; Email: qiong_wu@jlu.edu.cn

Daqian Song − *College of Chemistry, Jilin Province Research Center for Engineering and Technology of Spectral Analytical Instruments, Jilin University, Changchun 130012, China*; orcid.org/0000-0002-4866-1292; Email: songdq@jlu.edu.cn

Authors

Dianfeng Dai − *College of Chemistry, Jilin Province Research Center for Engineering and Technology of Spectral Analytical Instruments, Jilin University, Changchun 130012, China*

Zhimin Zhang − *Department of Pharmacy, Changchun Medical College, Changchun 130031, China*

Mo Ma − *College of Chemistry, Jilin Province Research Center for Engineering and Technology of Spectral Analytical Instruments, Jilin University, Changchun 130012, China; School of Pharmacy, Jilin University, Changchun 130012, China*

Chen Zhao − *College of Chemistry, Jilin Province Research Center for Engineering and Technology of Spectral Analytical Instruments, Jilin University, Changchun 130012, China*

Jingkang Li − *College of Chemistry, Jilin Province Research Center for Engineering and Technology of Spectral Analytical Instruments, Jilin University, Changchun 130012, China*

https://doi.org/10.1021/acs.analchem.5c00658
Anal. Chem. 2025, 97, 9414−9421

Siqi Zhang − *College of Chemistry, Jilin Province Research Center for Engineering and Technology of Spectral Analytical Instruments, Jilin University, Changchun 130012, China*

Complete contact information is available at: https://pubs.acs.org/10.1021/acs.analchem.5c00658

Notes

The authors declare no competing financial interest.

■ ACKNOWLEDGMENTS

This work was supported by the National Natural Science Foundation of China (22074052 and 22004046) and the Science and Technology Developing Foundation of Jilin Province of China (20230204116YY).

■ REFERENCES

(1) Medzhitov, R. *Science* **2021**, *374*, 1070−1075.
(2) Netea, M. G.; Balkwill, F.; Chonchol, M.; Cominelli, F.; Donath, M. Y.; Giamarellos-Bourboulis, E. J.; Golenbock, D.; Gresnigt, M. S.; Heneka, M. T.; Hoffman, H. M.; Hotchkiss, R.; Joosten, L. A. B.; Kastner, D. L.; Korte, M.; Latz, E.; Libby, P.; Mandrup-Poulsen, T.; Mantovani, A.; Mills, K. H. G.; Nowak, K. L.; O'Neill, L. A.; Pickkers, P.; van der Poll, T.; Ridker, P. M.; Schalkwijk, J.; Schwartz, D. A.; Siegmund, B.; Steer, C. J.; Tilg, H.; van der Meer, J. W. M.; van de Veerdonk, F. L.; Dinarello, C. A. *Nat. Immunol.* **2017**, *18*, 826−831.
(3) Hammerich, L.; Tacke, F. *Nat. Rev. Gastroenterol. Hepatol.* **2023**, *20*, 633−646.
(4) Solier, S.; Muller, S.; Caneque, T.; Versini, A.; Mansart, A.; Sindikubwabo, F.; Baron, L.; Emam, L.; Gestraud, P.; Pantos, G. D.; Gandon, V.; Gaillet, C.; Wu, T. D.; Dingli, F.; Loew, D.; Baulande, S.; Durand, S.; Sencio, V.; Robil, C.; Trottein, F.; Pericat, D.; Naser, E.; Cougoule, C.; Meunier, E.; Begue, A. L.; Salmon, H.; Manel, N.; Puisieux, A.; Watson, S.; Dawson, M. A.; Servant, N.; Kroemer, G.; Annane, D.; Rodriguez, R. *Nature* **2023**, *617*, 386−394.
(5) Karin, M.; Clevers, H. *Nature* **2016**, *529*, 307−315.
(6) Wang, X.; Ding, Q.; Groleau, R. R.; Wu, L.; Mao, Y.; Che, F.; Kotova, O.; Scanlan, E. M.; Lewis, S. E.; Li, P.; Tang, B.; James, T. D.; Gunnlaugsson, T. *Chem. Rev.* **2024**, *124*, 7106−7164.
(7) Dolinger, M.; Torres, J.; Vermeire, S. *Lancet* **2024**, *403*, 1177−1191.
(8) Sands, B. E. *Gastroenterology* **2015**, *149*, 1275−1285.e1272.
(9) Fredman, G.; Serhan, C. N. *Nat. Rev. Cardiol.* **2024**, *21*, 808−823.
(10) Tu, J.; Min, J.; Song, Y.; Xu, C.; Li, J.; Moore, J.; Hanson, J.; Hu, E.; Parimon, T.; Wang, T.-Y.; Davoodi, E.; Chou, T.-F.; Chen, P.; Hsu, J. J.; Rossiter, H. B.; Gao, W. *Nat. Biomed. Eng.* **2023**, *7*, 1293−1306.
(11) Cui, W. L.; Wang, M. H.; Yang, Y. H.; Wang, J. Y.; Zhu, X. Z.; Zhang, H. T.; Ji, X. X. *Coordin. Chem. Rev.* **2023**, *474*, No. 214848.
(12) Duo, Y.; Han, L.; Yang, Y.; Wang, Z.; Wang, L.; Chen, J.; Xiang, Z.; Yoon, J.; Luo, G.; Tang, B. Z. *Chem. Rev.* **2024**, *124*, 11242−11347.
(13) Zhou, M.; Liang, S.; Liu, D.; Ma, K.; Peng, Y.; Wang, Z. *ACS Nano* **2022**, *16*, 19940−19958.
(14) Russell, W. M.; Klaenhammer, T. R. *Appl. Environ. Microb.* **2001**, *67*, 1253−1261.
(15) Lietzan, A. D.; Simpson, J. B.; Walton, W. G.; Jariwala, P. B.; Xu, Y.; Boynton, M. H.; Liu, J.; Redinbo, M. R. *Sci. Adv.* **2023**, *9*, No. eadg3390.
(16) Rosay, T.; Jimenez, A. G.; Sperandio, V. *Proc. Natl. Acad. Sci. U.S.A.* **2024**, *121*, No. e2400226121.
(17) Pellock, S. J.; Redinbo, M. R. *J. Biol. Chem.* **2017**, *292*, 8569−8576.
(18) Bramwell, K. K.; Ma, Y.; Weis, J. H.; Chen, X.; Zachary, J. F.; Teuscher, C.; Weis, J. J. *J. Clin. Invest.* **2014**, *124*, 311−320.
(19) Rutenburg, A. M.; Pineda, E. P.; Banks, B. M.; Goldbarg, J. A. *Am. J. Dig. Dis.* **1963**, *8*, 789−797.
(20) Shimoi, K.; Nakayama, T. *Methods Enzymol.* **2005**, *400*, 263−272.
(21) Awolade, P.; Cele, N.; Kerru, N.; Gummidi, L.; Oluwakemi, E.; Singh, P. *Eur. J. Med. Chem.* **2020**, *187*, No. 111921.
(22) Lampe, J. W.; Li, S. S.; Potter, J. D.; King, I. B. *J. Nutr.* **2002**, *132*, 1341−1344.
(23) Boyland, E.; Wallace, D. M.; Williams, D. C. *Br. J. Cancer* **1955**, *9*, 62−79.
(24) Yang, S.; McGookey, M.; Wang, Y.; Cataland, S. R.; Wu, H. M. *Am. J. Clin. Pathol.* **2015**, *143*, 558−565.
(25) Keating, J.; Tchou, J.; Okusanya, O.; Fisher, C.; Batiste, R.; Jiang, J.; Kennedy, G.; Nie, S.; Singhal, S. *J. Surg. Oncol.* **2016**, *113*, 508−514.
(26) Ellis, K. J. *Physiol. Rev.* **2000**, *80*, 649−680.
(27) Zhang, W.; Liu, J.; Li, P.; Wang, X.; Tang, B. *Acc. Chem. Res.* **2024**, *57*, 2594−2605.
(28) Meng, W.; Chen, R.; Jang, Q.; Ma, K.; Li, D.; Xiao, H.; Chi, W.; Zeng, C.; Shu, W. *Coordin. Chem. Rev.* **2025**, *529*, No. 216456.
(29) Quan, W.; Song, W.; Zhang, Q.; Huang, H.; Lin, W. *Coordin. Chem. Rev.* **2023**, *497*, No. 215407.
(30) Ye, Y. X.; Pan, J. C.; Wang, H. C.; Zhang, X. T.; Zhu, H. L.; Liu, X. H. *Chem. Soc. Rev.* **2024**, *53*, 9133−9189.
(31) Cheng, T. C.; Roffler, S. R.; Tzou, S. C.; Chuang, K. H.; Su, Y. C.; Chuang, C. H.; Kao, C. H.; Chen, C. S.; Harn, I. H.; Liu, K. Y.; Cheng, T. L.; Leu, Y. L. *J. Am. Chem. Soc.* **2012**, *134*, 3103−3110.
(32) Lou, X.; Ren, T. B.; Chen, H.; Huan, S. Y.; Yuan, L.; Zhang, X. B. *Biomaterials* **2022**, *287*, No. 121657.
(33) Jin, Y.; Tian, X.; Jin, L.; Cui, Y.; Liu, T.; Yu, Z.; Huo, X.; Cui, J.; Sun, C.; Wang, C.; Ning, J.; Zhang, B.; Feng, L.; Ma, X. *Anal. Chem.* **2018**, *90*, 3276−3283.
(34) Wei, X.; Hao, M.; Hu, X.-X.; Song, Z.; Wang, Y.; Sun, R.; Zhang, J.; Yan, M.; Ding, B.; Yu, J. *Sens. Actuators, B* **2021**, *326*, No. 128849.
(35) Wang, J.; Zhang, L.; Su, Y.; Qu, Y.; Cao, Y.; Qin, W.; Liu, Y. *Anal. Chem.* **2022**, *94*, 7012−7020.
(36) Shang, J.; Zhang, X.; He, Z.; Shen, S.; Liu, D.; Shi, W.; Ma, H. *Angew. Chem., Int. Ed.* **2022**, *61*, No. e202205043.
(37) Jiang, G.; Liu, H.; Deng, G.; Liu, H.; Zhou, Z.; Ren, T. B.; Wang, L.; Zhang, X. B.; Yuan, L. *Angew. Chem., Int. Ed.* **2024**, *63*, No. e202400637.
(38) Alivernini, S.; Firestein, G. S.; McInnes, I. B. *Immunity* **2022**, *55*, 2255−2270.
(39) Zhang, Y.; Liu, D.; Chen, W.; Tao, Y.; Li, W.; Qi, J. *Adv. Mater.* **2024**, *36*, No. e2409661.
(40) Pancewicz, S.; Popko, J.; Rutkowski, R.; Knas, M.; Grygorczuk, S.; Guszczyn, T.; Bruczko, M.; Szajda, S.; Zajkowska, J.; Kondrusik, M.; Sierakowski, S.; Zwierz, K. *Scand. J. Infect. Dis.* **2009**, *41*, 584−589.
(41) El-Shiekh, R. A.; El-Mekkawy, S.; Mouneir, S. M.; Hassan, A.; Abdel-Sattar, E. *J. Ethnopharmacol.* **2021**, *270*, 113779.
(42) Mieli-Vergani, G.; Vergani, D.; Czaja, A. J.; Manns, M. P.; Krawitt, E. L.; Vierling, J. M.; Lohse, A. W.; Montano-Loza, A. J. *Nat. Rev. Dis. Primers.* **2018**, *4*, No. 18017.
(43) European Association for the Study of the, Liver. *J. Hepatol.* **2015**, *63*, 971−1004.
(44) Baumgart, D. C.; Carding, S. R. *Lancet* **2007**, *369*, 1627−1640.
(45) Nikolaus, S.; Schreiber, S. *Gastroenterology* **2007**, *133*, 1670−1689.